Available online at www.sciencedirect.com
ScienceDirect
Progress in Natural Science 18 (2008) 999–1007
Progress in Natural Science
www.elsevier.com/locate/pnsc

Molecular dynamics simulations of non-Fourier heat conduction

Qixin Liu, Peixue Jiang *, Heng Xiang

Key Laboratory for Thermal Science and Power Engineering of Ministry of Education, Department of Thermal Engineering, Tsinghua University, Beijing 100084, China

Received 23 October 2007; received in revised form 20 February 2008; accepted 22 February 2008

Abstract

Unsteady heat conduction is known to deviate significantly from Fourier's law when the system time and length scales are within certain temporal and spatial windows of relaxation. Classical molecular dynamics simulations were used to investigate unsteady heat conduction in argon thin films with a sudden temperature increase or heat flux at one surface to study the non-Fourier heat conduction effects in argon thin films. The studies were conducted with both pure argon films and films with vacancy defects. The temperature profiles in the argon films showed the existence of mechanical waves when the thin film was suddenly heated and the wave nature of the heat propagation. The flux phase relaxation time, τ_q, and the temperature phase relaxation time, τ_t, were calculated from the temporal variations of the energy flux and temperature distribution in the film. Comparisons of the MD temperature profiles with temperature profiles predicted by Fourier's law show that Fourier's law is not able to predict the temperature variations with time. Different film thicknesses were also studied to illustrate the variation of the time needed for the films to reach steady-state temperature profiles after a sudden temperature rise at one surface and to illustrate the finite speed of the energy waves.

Keywords: Molecular dynamics simulation; Non-Fourier heat conduction; Argon thin film

1. Introduction

New technologies are developing in the direction of smaller scales. Many commonly used devices such as personal computers involve microelements, which operate on nanosecond time scales, at which energy transported along distances on the order of a single atom. Nanoscale dielectric films are now important components of many microelectronic and photoelectronic devices. The analysis of the thermal conduction in dielectric films is very important for the design of microelectronic and photoelectronic devices. Better understanding of the laws that govern physical processes on such scales is necessary. Therefore, the thermal characteristics of microscale and nanoscale components, especially thin films, have been a key focus of international heat transfer research in the past two decades [1,2]. The deviation of nonstationary heat conduction from Fourier's law is known to become significant when the system time and length scales are within certain temporal and spatial windows of relaxation [3]. A consequence of Fourier's phenomenological law

$$q_{\mathrm{F}} = -\lambda \cdot \nabla T \tag{1}$$

is that the heat velocity is infinite as pointed out by Cattaneo and Vernotte [4,5]. Therefore, they proposed that a more realistic assumption would be that the heat flux evolves according to the relaxation law

$$\frac{\mathrm{d}q}{\mathrm{d}t} = \frac{q_{\mathrm{F}} - q}{\tau_V} \tag{2}$$

where τ_V is the relaxation time of the non-Fourier process. Introducing Eq. (2) into the energy conservation equation gives the hyperbolic heat conduction equation which can be written in one dimension as

* Corresponding author. Tel.: +86 10 62772661; fax: +86 10 62770209.
E-mail address: Jiangpx@tsinghua.edu.cn (P. Jiang).

1002-0071/$ - see front matter
doi:10.1016/j.pnsc.2008.05.001

$$\frac{\partial T}{\partial t}+\tau_V\frac{\partial^2 T}{\partial^2 t}=\alpha\frac{\partial^2 T}{\partial^2 x} \tag{3}$$

where α is the thermal diffusivity. Tzou [6] proposed a dual phase lag model with Fourier's law modified as

$$\vec{q}(t+\tau_q,\vec{r})=-k\nabla T(t+\tau_t,\vec{r}) \tag{4}$$

where τ_q and τ_t are the heat flux and temperature phase relaxation times. Combining Eq. (4) with the energy conservation law gives the dual phase lag model in one dimension:

$$\frac{\partial T}{\partial t}+\tau_q\frac{\partial^2 T}{\partial t^2}=\alpha\left[\nabla^2 T+\tau_t\frac{\partial(\nabla^2 T)}{\partial t}\right]. \tag{5}$$

At the limit of $\tau_t=0$, this expression reduces to Eq. (3).

Classical molecular dynamics (MD) simulations have already been widely used to study nanoscale thermal conduction. In MD methods, the positions and momentum space trajectories of a system of particles are calculated by solving Newton's equation of motion for all the particles. Besides the potential mode, no assumptions are needed to simulate the heat transfer. Studies [7,8] of non-Fourier heat conduction in single-walled carbon nanotubes using classical MD simulations have shown non-Fourier heat conduction effects where a distinct amount of heat is transported in a wavelike form. Other molecular dynamics simulations of heat pulse propagation in single-walled carbon nanotubes [9] showed that picosecond heat pulses in (10,0), (7,0), and (5,5) single-walled carbon nanotubes induce several wave packets that propagate at different propagation speeds. MD simulations of the thermal response of a silicon crystal irradiated by a pico-femto heat pulse [10] showed significant differences from classical predictions. These studies focused on single-walled carbon nanotubes and silicon crystals in which the heat conduction is not solely by phonons. Sebastian et al. [11] studied transient heat conduction in solid argon films with MD simulations, but their study only focused on the transient heat conduction due to sudden temperature changes on one end of pure film. Real crystals always contain defects such as impurities, vacancies, and dislocations, which reduce the thermal conduction due to phonon scattering by the defects. To our knowledge, no papers have reported studies on non-Fourier heat conduction in argon thin films with defects. This paper presents a study of non-Fourier heat conduction in pure argon thin films and films with vacancy defects using classical molecular dynamics simulations. The film is assumed to be subjected to a local temperature change or heat flux at one end with the resulting temperature changes analyzed to study the heat conduction in the film. The results illustrate the wave nature of the thermal conduction and the temperature lag. Argon films were analyzed because the energy conduction in such films is dominated by phonon transport and also because of the availability of a good intermolecular potential for argon. The widely accepted Lennard–Jones 12–6 (L–J) potential matches experimental data for bulk argon reasonably well.

2. MD simulation method

The geometry used for the MD simulations is sketched in Fig. 1. It consists of "fixed", "hot", "regular", "cold", and "fixed" sections. The fixed atoms are stationary during the whole simulation and serve as adiabatic boundary conditions. The "hot" and "cold" atoms are temperature control boundary zones where the velocities of each atom are controlled to maintain the desired temperature. In the regular section, the molecular motion is based solely on the L–J potential mode. The "fixed" section is three lattice layers thick, and the "hot" and "cold" sections are four lattice layers thick, while the thickness of the "regular" section is changeable to vary the thickness of the whole film. Periodic boundary conditions are used in the z and y directions. The interaction between atoms is described by the Lennard–Jones (6–12) pair potential which is written as

$$\phi(r_{i,j})=4\varepsilon\left[\left(\frac{\delta}{r_{i,j}}\right)^{12}-\left(\frac{\delta}{r_{i,j}}\right)^{6}\right] \tag{6}$$

where $r_{i,j}$ is the distance between atoms i and j, ε is the well-depth parameter whose value is 1.67×10^{-21} J and δ is the equilibrium separation parameter whose value is 3.405×10^{-10} m. Only the neighbors of each atom within a certain cutoff radius, 2.6 $\delta_{\mathrm{L-J}}$, were included in the force calculations because far away atoms have negligible effect on the total force. The standard L–J dimensionless length, temperature and energy were used in the simulations. The spatial temperature distribution in the film was obtained by dividing the entire film into layers along the x direction. The number of layers depends on the film thickness with a maximum of 5760 atoms simulated. The temperature of each layer was usually defined as

$$T=\frac{\sum_{i=1}^{N} m_i v_i^2}{3Nk_{\mathrm{B}}} \tag{7}$$

where N is the number of atoms in the layer. At the beginning of each run, all the nonfixed atoms were given an initial temperature of 10 K by choosing their velocities based on the Maxwell distribution. Then, the whole film was kept at this temperature for 1 ns to reach equilibrium. The film was then run at the NVE ensemble for another 2 ns. Then, the temperature of the "hot" section was raised to a higher temperature, while the temperature of the "cold" section was maintained constant to study the heat flux phase relax-

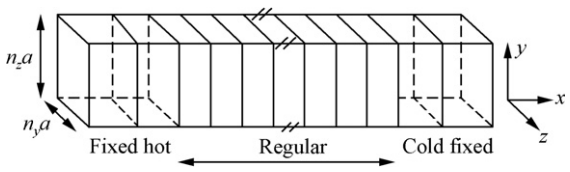

Fig. 1. Simulation model.

ation time or the "hot" section work as the constant energy flux boundary condition to study the temperature phase relaxation time.

3. MD simulation results

3.1. Wave nature of thermal conduction in pure films

The spatial temperature distribution along the film after the "hot" section temperature was suddenly changed to 80 K is shown in Fig. 2 for a 20 nm thick film. The sudden increase of the "hot" section temperature results in thermal expansion [11], which creates mechanical waves. Since both the mechanical and thermal waves occur as atomic vibrations, the effects of the mechanical wave on the temperature need to be studied. We distinguish the mechanical wave from the atom's kinetic energy by redefining the temperature of each film layer as [11]

$$\frac{3}{2}Nk_{\mathrm{B}}T_{\mathrm{a}} = \sum_{i=1}^{N}\frac{1}{2}m(v_i - u)^2 \tag{8}$$

where T_{a} means the actual temperature and u is the mean velocity of the atoms in each film layer. This definition reflects that the mechanical expansion behaves as the atoms group movement, so the mean velocity of the atoms in each film layer is subtracted from the total energy.

The spatial superficial and actual temperature distributions without the effect of the mechanical wave are compared first. Fig. 2 shows that the effect of the mechanical wave obviously exists because there is a difference between the superficial temperature distribution and the actual temperature distribution when the effects of the mechanical wave are re-

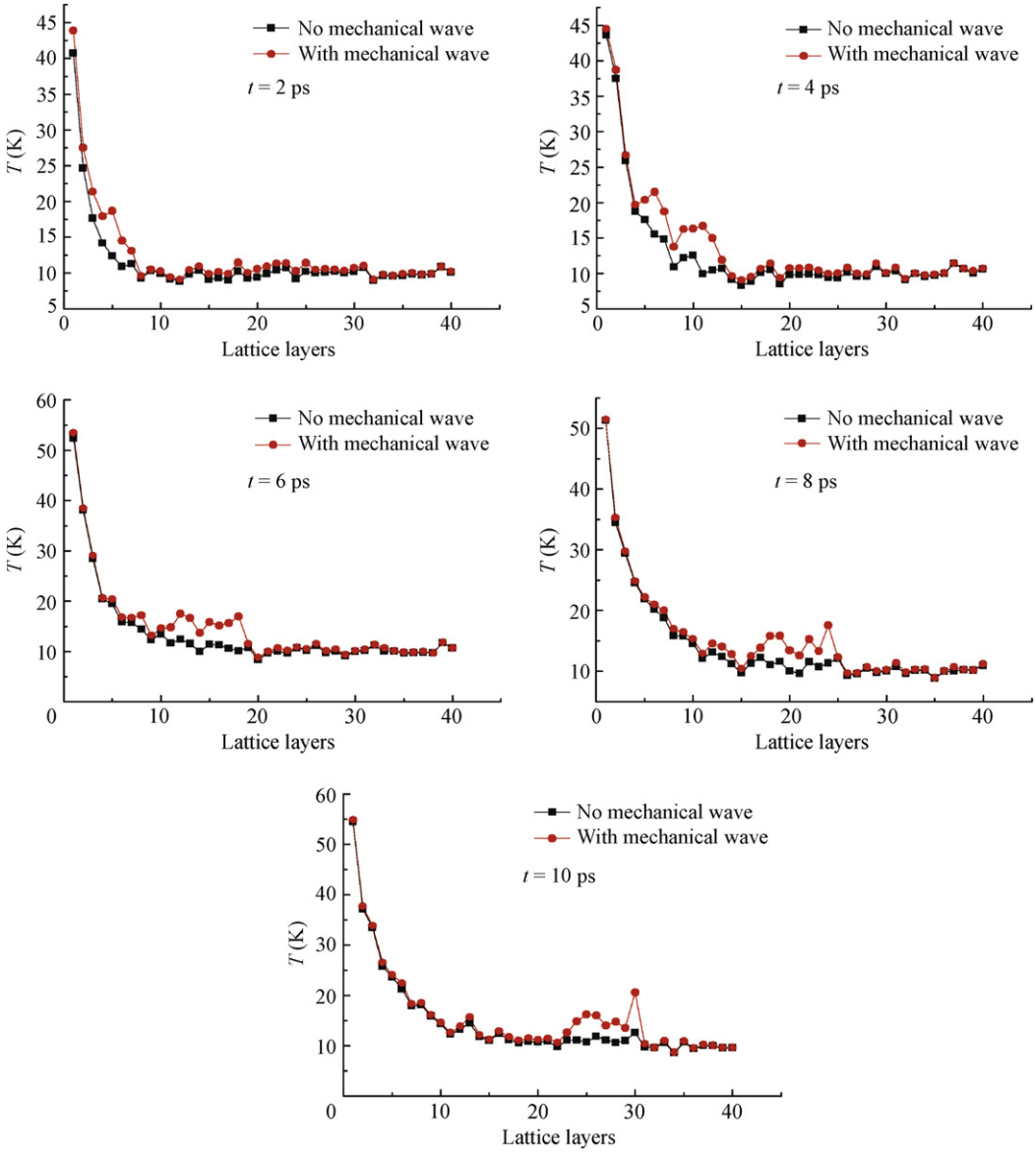

Fig. 2. Comparison between the superficial and actual temperature distributions after a temperature change is applied to a pure thin film.

moved. The difference can be seen moving across the film thickness. The superficial and actual temperature distributions in areas not affected by the mechanical wave are identical. These results illustrate that the mechanical wave, unlike the thermal wave, is only generated at the beginning of the temperature increase. The speed of the mechanical wave calculated from the temperature distribution is about 1800 m/s, which approaches the sound speed at that temperature.

The sudden temperature increase at one end of the film also induces clearly defined thermal waves that propagate through the argon film. Fig. 3 shows the actual temperature distribution in the argon thin film after the "hot" end of the thin film was suddenly raised to 80 K. The wave nature of the heat transfer in the argon film can be seen in waves 1, 2, and 3 in Fig. 3 moving towards the low temperature end. The results also show that the thermal waves move at different speeds at different times. For example, from 2 to 4 ps, wave 2 moved about 1.5 nm; however, from 4 to 6 ps it moved only about 0.8 nm due to interactions with the other wave which correspond to phonon interactions [12].

3.2. Wave nature of thermal conduction in films with vacancy defects

Real crystals always contain defects such as impurities, vacancies and dislocations, which reduce the thermal conduction due to phonon scattering by the defects. In our former paper [13], we used molecular dynamics simulations to study the thermal conductivities of films with vacancy defects. Our results showed that the thermal conductivities of films with vacancy defects are lower than those of perfect films with the same thickness. Since the thermal conductivity is related to the thermal waves, the effects of these vacancy defects on the thermal waves in films need to be further understood. Here, the vacancies were modeled as defects to avoid the difficulties of different potential models with defects caused by different materials. The difference between simulations for films with vacancy defects and simulations with pure films lies only in the initial construction of films with vacancy defects. The vacancies in the film were formed by randomly removing a selected number of atoms from perfect argon FCC lattices.

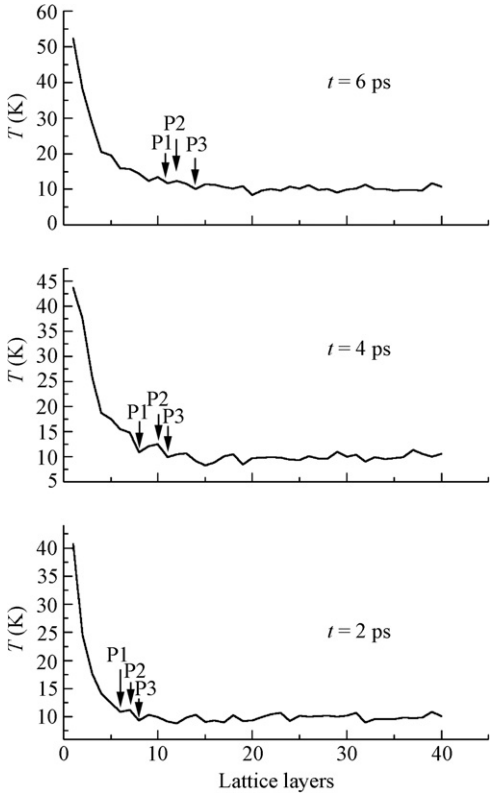

Fig. 3. Actual temperature distribution in a 20-nm thick argon film with the "hot" section temperature suddenly increased to 80 K.

Fig. 4 shows the spatial temperature distribution in a 20 nm thick argon film with 56 vacancy defects. As with the pure films, mechanical and thermal waves are seen to propagate through the film. Comparison of Figs. 2 and 4 shows that there is no significant difference between the mechanical wave propagation in films with and without vacancy defects. Fig. 5 shows that like the mechanical wave, the thermal wave propagation in films with vacancy defects does not differ from the wave propagation in pure films. According to the kinetic theory of phonon gases, the thermal conductivity of the solid state is given by

$$k = \frac{1}{3} c_v v^2 \tau \tag{9}$$

where c_v is the specific heat per unit volume, v is the average speed of the thermal waves and τ is the mean time between phonon scattering events. Thus, the reduction of the film thermal conductivity due to vacancy defects is mainly caused by the reduction of τ.

3.3. Heat flux relaxation time for pure films

One of the most important characteristics of non-Fourier thermal conduction is the lag between the heat flux and temperature gradient since τ_q is not equal to zero. The energy flux in the each layer of the film was calculated as

$$J_h = \sum_{j=1}^{N} \left(E_j v_j + \frac{1}{2} \sum_{i \neq j}^{N} r_{ij} F_{ij} \cdot v_j \right) \tag{10}$$

where J_h is the energy flux in the hth lattice layer with E_j defined by the energy of particle j,

$$E_j = \frac{1}{2} m v_j^2 + \frac{1}{2} \sum_{i \neq j}^{N} u(r_{ij}) \tag{11}$$

where v_j is the particle velocity and F_{ij} is the intermolecular force between particles i and j. When the film temperature at one end is suddenly raised, the energy flux lags behind the temperature gradient. The energy flux in each film layer at different times is compared with actual temperature distributions to obtain the time interval

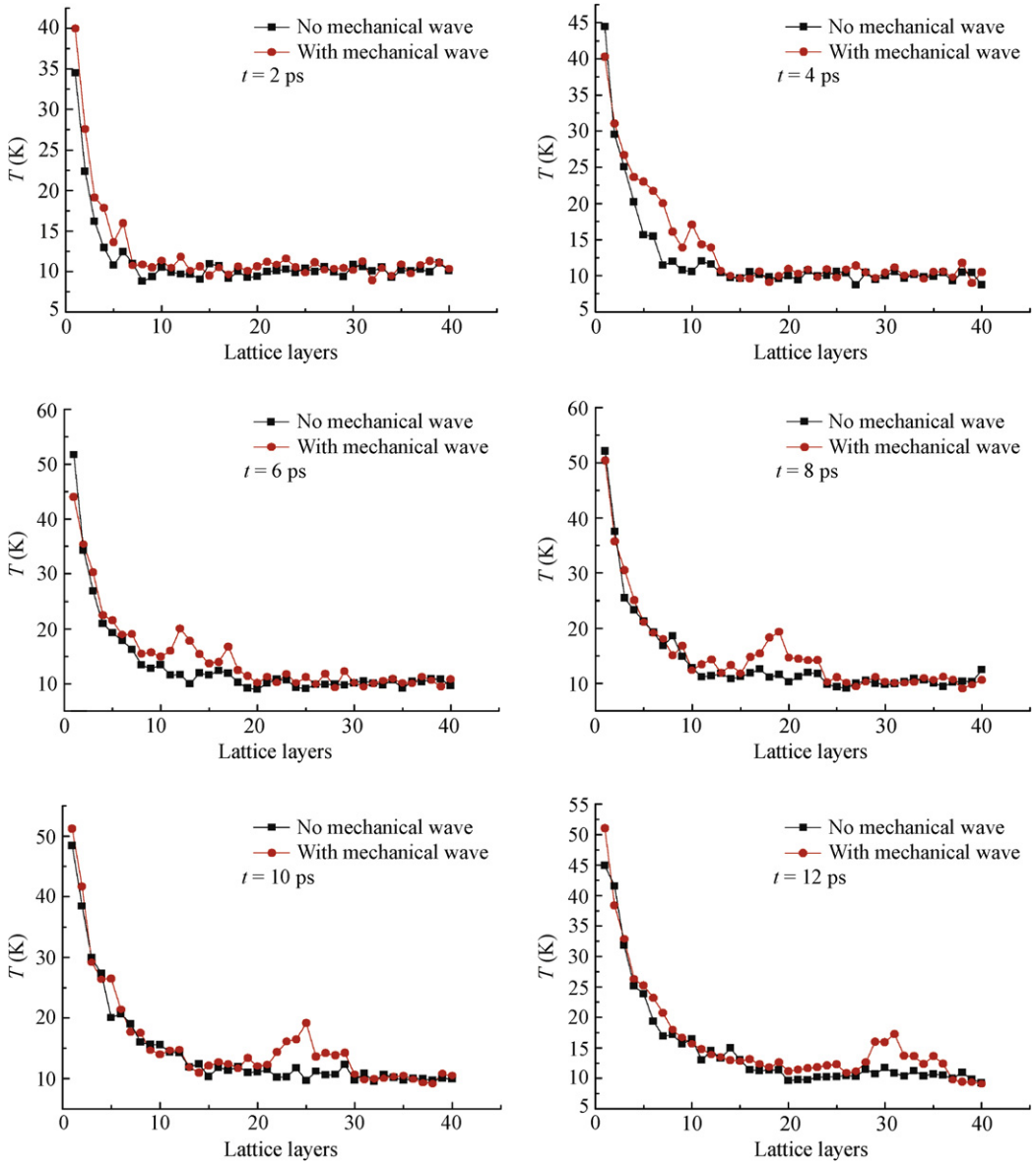

Fig. 4. Comparison between the superficial and actual temperature distributions after a temperature change was applied to one end of a 20-nm thin film with 56 defects.

at which the energy flux and the temperature gradient overlapped, τ_q can then be obtained. For the temperature distribution in Fig. 3, τ_q is 30 ps.

The actual temperature distributions in the argon film were also used to estimate the time at which the temperature becomes stable. Fig. 6 shows the temperature distribution variation with time in a 10 nm thick pure film, with that for a 20 nm thick pure film shown in Fig. 7.

The temperature distribution in the 10 nm thick argon film needed about 80 ps to reach steady-state, while for the 20 nm thick film the time was about 300 ps. Thus, the temperature distributions in thicker films take longer to reach steady-state than in thinner films as expected with the final steady-state temperature distribution which is similar to the Fourier's law based temperature distribution. The increased time predicted by the MD simulations for the thicker argon film temperature to reach steady-state illustrates the finite speed of the energy wave.

After the sudden temperature rise was applied to the film, the film undergoes transient heating which can be modeled using the classical Fourier's law by numerically solving the one-dimensional Fourier's law based thermal conduction equation. For the 10 nm thick argon film, the temperature distribution becomes stable after 12 ps, which is much shorter than that predicted by the MD simulation, with the 20 nm thick argon film requiring 25 ps.

Table 1 compares the predicted steady-state times from the MD and Fourier's law analyses for other films. These results show that for nanoscale argon films, the thermal conduction process is very non-Fourier, with the predicted

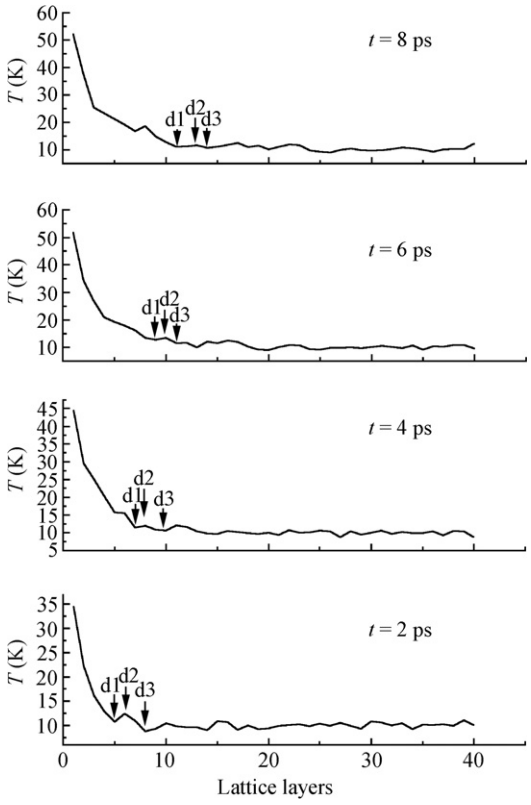

Fig. 5. Actual temperature distributions in a 20-nm thick argon film with vacancy defects.

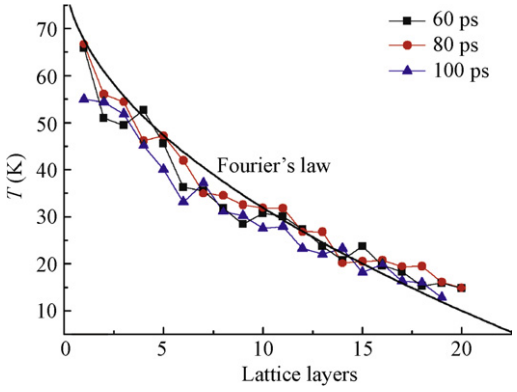

Fig. 6. Temperature distribution in a 10-nm thick film.

times from the MD simulations being much longer than from the Fourier's law analysis.

3.4. Heat flux relaxation time for films with vacancy defects

As with pure films, τ_q in films with defects can be calculated by comparing the energy flux and temperature distributions. In these tests, τ_q was found to be nearly the same in the film with defects as in pure film.

The temperature distribution variation in a 10 nm thick film with 14 vacancy defects is shown in Fig. 8, with that for a 20 nm thick film with 28 vacancy defects shown in Fig. 9. As with the pure films, the thicker films require longer time to reach steady-state with the steady-state temperature distributions in both films being essentially equal to the Fourier-based distribution. The time to steady-state

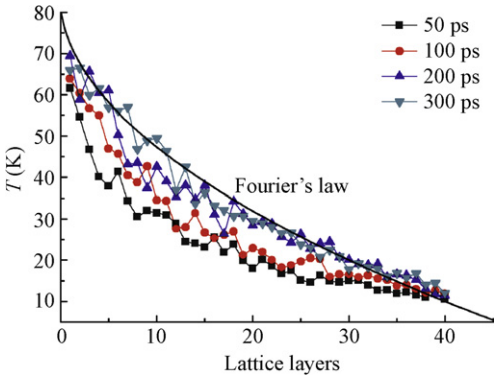

Fig. 7. Temperature distribution in a 20-nm thick film.

Table 1
Variation of the time to reach steady-state in pure films

Film thickness (nm)	15	25
Time based on MD (ps)	170	400
Time based on Fourier's law (ps)	19	32

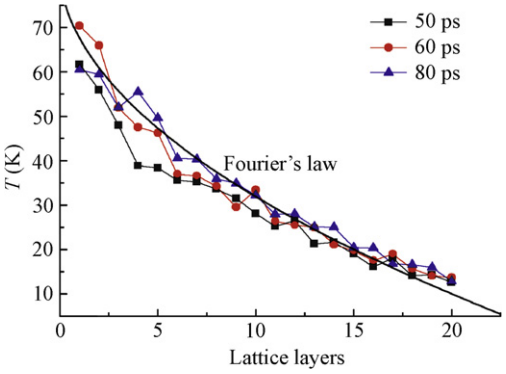

Fig. 8. Temperature distributions in a 10-nm thick film with 14 vacancy defects.

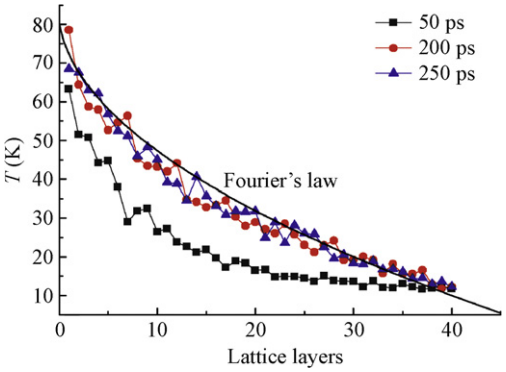

Fig. 9. Temperature distributions in a 20-nm thick film with 28 vacancy defects.

for the 10 nm thick film with 14 vacancy defects was about 60 ps and for the 20 nm thick film with 28 vacancy defects was about 250 ps, which are nearly the same as for the pure films with the same thicknesses. Thus, the energy wave propagation speeds are essentially the same with and without defects.

4. Temperature phase relaxation time of pure films

The previous results used a sudden change in the temperature of one end of the film to determine the heat flux phase relaxation time, τ_q. A constant energy flux can also be applied to one end of the film by changing the velocities of the atoms with "hot" section while recording the film temperatures to study the temperature phase relaxation time.

Fig. 10 shows the spatial temperature distributions in a 20-nm thick film with a constant energy flux of 1.995×10^8 W/m^2. After the energy flux was applied to the film, the temperatures near the "hot" atoms first began to increase with the temperatures near the "hot" atoms continuing to increase and the point at which the temperature start to change moves towards the "cold" section. The temperature of the rest of the film was still about 10 K. Fig. 11 shows the spatial temperature distribution in the 20-nm thick film with a constant energy flux of 0.997×10^8 W/m^2.

Comparison between Figs. 10 and 11 shows that the speed of the temperature change in the film is lower with the decreased energy flux. For example, when the energy flux is 0.997×10^8 W/m^2 the region affected by the energy flux of 16 ps after beginning is nearly the same as the region affected by the 1.995×10^8 W/m^2 energy flux after 6 ps. Thus, the energy translation speed in the film is finite.

As mentioned before, when the film experiences a constant energy flux boundary condition, the temperature distribution lags the energy flux, so the temperature phase relaxation time, τ_t, can be calculated by comparing the energy flux and temperature distributions as before. The results show that τ_t of the 10 nm thick argon film is about 4 ps, which is shorter than τ_q.

The constant heat flux boundary condition MD results in Fig. 11 can also be compared with the Fourier-based results in Fig. 12. Fig. 12 shows the temperature distribution predicted by the Fourier equation 12 ps after an energy flux of 0.995×10^8 W/m^2 was applied to a 20-nm thick film. The temperature distribution in Fig. 12 differs greatly from the corresponding distribution in Fig. 11. Fig. 12 shows that the entire film is affected by the energy flux and the temperature difference across the film is only 2.5 °C, which is much smaller than the MD results where the temperature difference across the film is almost 10 °C. Thus, the Fourier model has no lag between the temperature gradient and the energy flux. These phenomena illustrate the importance of the non-Fourier heat transfer effects in nanoscale thin films.

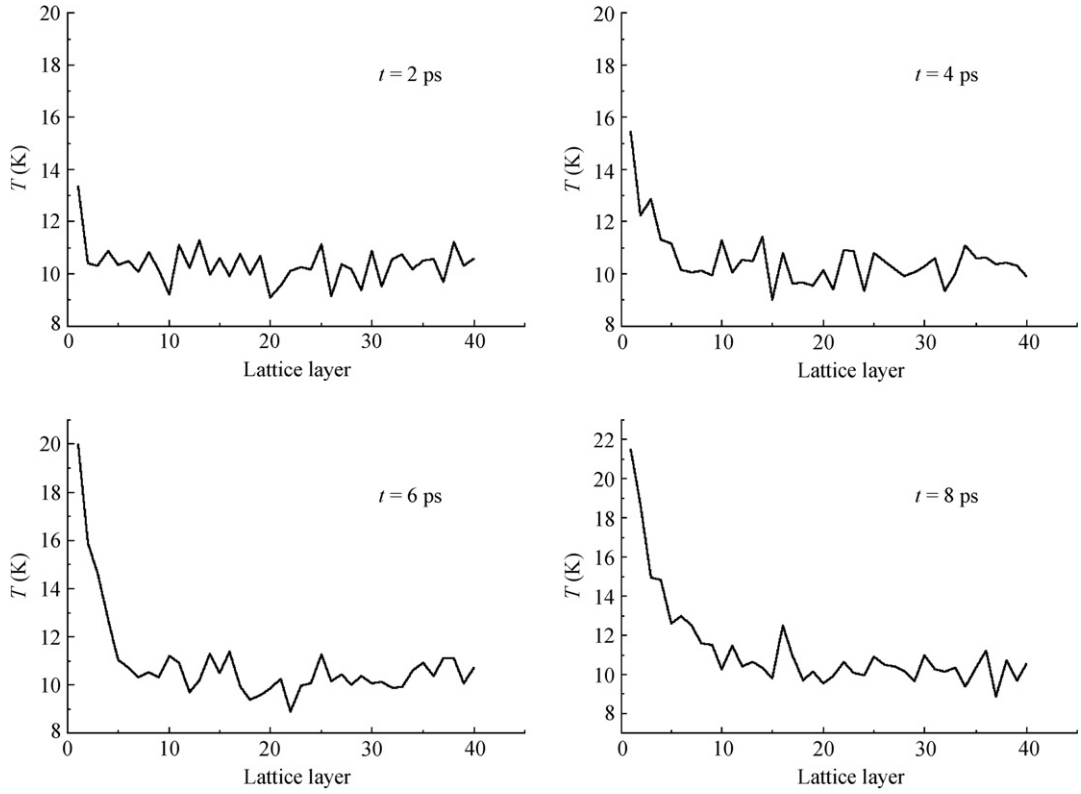

Fig. 10. Spatial temperature distributions in a film with a constant energy flux of 1.995×10^8 W/m^2.

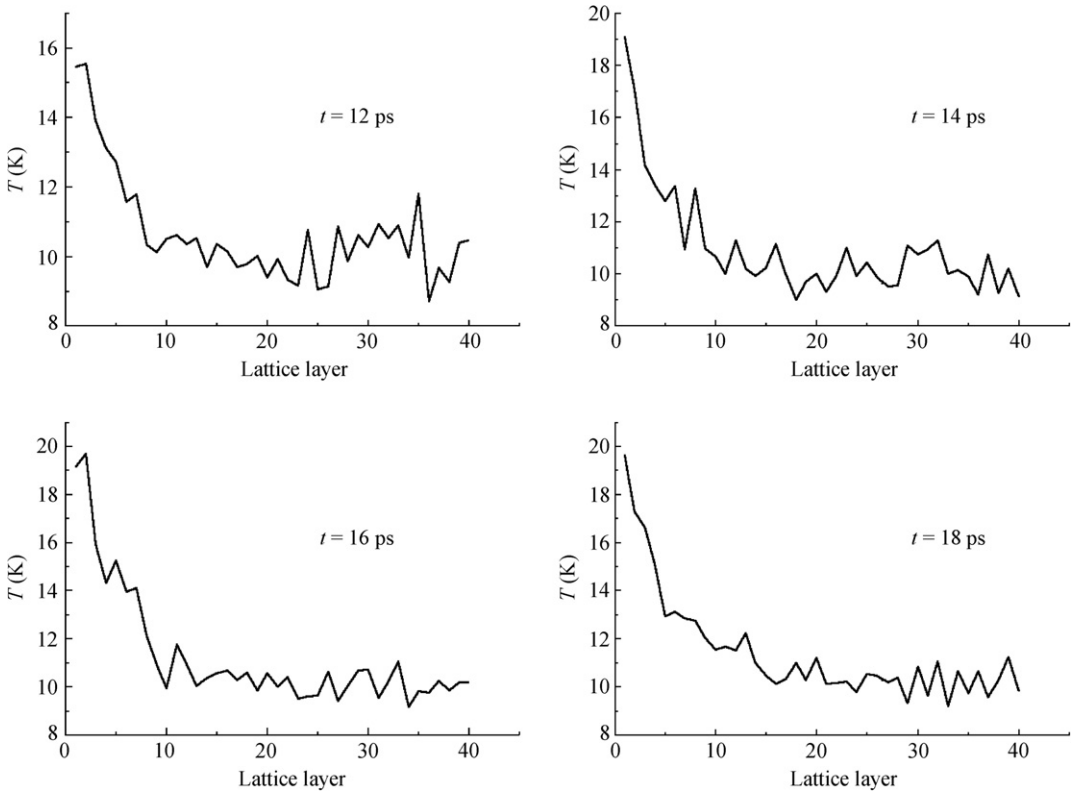

Fig. 11. Spatial temperature distributions in a film with a constant energy flux of 0.997×10^8 W/m^2.

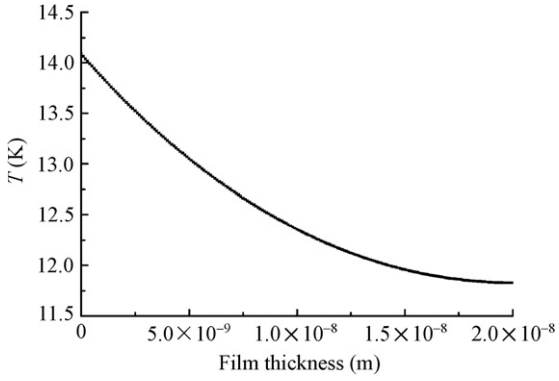

Fig. 12. Fourier temperature 12 ps after an energy flux of 0.995×10^8 W/m^2 was applied to a 20-nm film.

5. Conclusions

Classic molecular dynamics simulations were used to analyze unsteady thermal conduction in argon thin films subjected to temperature increase or energy fluxes at one surface to study the non-Fourier heat conduction effects in argon thin films. The study considered pure argon films and argon films with vacancy defects. The results show the wave nature of the thermal conduction in the argon thin films with the thermal waves affecting each other as they propagate. The MD simulations show that the thermal wave speeds in films with vacancy defects are essentially the same as the wave speeds in pure films.

The flux phase relaxation time, τ_q, and temperature phase relaxation time, τ_t, were calculated by comparing the energy flux and temperature distributions in the film after the film was subjected to a sudden temperature rise and a sudden energy flux increase at one end. τ_q was found to be the same in the pure films as in films with vacancy defects and τ_t was found to be smaller than τ_q. The MD simulations also show that when applying a sudden temperature increase to the thin film, some time is needed for the film temperature distribution to reach steady-state and this time is much larger than that predicted by Fourier's law. The temperature distributions predicted by the MD analysis in a thin film after an energy flux were applied to the film differed significantly from the Fourier results, thus, non-Fourier effects are quite significant in thin argon films.

Acknowledgments

This work was supported by the National Natural Science Foundation of China (Grant No. 50676047) and the Tsinghua Basic Research Foundation (Grant No. JCpy2005049).

References

[1] Tien CL, Chen G. Challenges in microscale conductive and radiative heat transfer. J Heat Transf 1994;116(4):799–807.
[2] Chou FC, Lukes JR, Liang XG. Molecular dynamics in microscale thermophysical engineering. Annu Rev Heat Transf 1999;10:141–76.

[3] Joseph DD, Preziosi L. Addendum to the paper "heat waves". Rev Mod Phys 1990;62:375–91.
[4] Vernotte PCR. Les paradoxes de la théorie continue de l'équation de la chaleur. Acad Sci (Paris) 1958;246:3154–5.
[5] Cattaneo CCR. Sur une forme de l'équation de la chaleur éliminant le paradoxe d'une propagation instantanée. Acad Sci (Paris) 1958;247:431–3.
[6] Tzou DY. A unified field approach for heat conduction form macro-to-micro-scales. J Heat Transf 1995;117:8–16.
[7] Shiomi J, Maruyama S. Non-Fourier heat conduction in a single-walled carbon nanotube: classical molecular dynamics simulations. Phys Rev B 2006;73:205420.
[8] Shiomi J, Maruyama S. Non-Fourier heat conduction of single-walled carbon nanotubes. Therm Sci Eng 2005;13(4):89–90.
[9] Mohamed AO, Deepak S. Molecular dynamics simulation of heat pulse propagation in single-walled carbon nanotubes. Phys Rev B 2005;72:125413.
[10] Sebastian V, Remi C, Karl J. Thermal response of silicon crystal to pico-femtosecond heat pulse by molecular dynamics. Microscale Therm Eng 2004;8:155–67.
[11] Sebastian V, Bernard SJ, Michel L. Transient Fourier-law deviation by molecular dynamics in solid argon. Phys Rev B 1996;54:340–7.
[12] Charles K. Introduction to solid state physics. 7th ed. New York: John Wiley and Sons Inc; 1996, p. 132–33.
[13] Liu QX, Jiang PX, Xiang H. Molecular dynamics study of the thermal conductivity of nanoscale argon films. Mol Simulat 2006;32(8):645–9.